

Investigation of low-temperature excitonic and defect emission from Ni-doped ZnO nanoneedles and V-doped ZnO nanostructured film

To cite this article: Shubra Singh *et al* 2010 *New J. Phys.* **12** 023007

View the [article online](#) for updates and enhancements.

Related content

- [Synthesis and optical properties of well aligned ZnO nanorods on GaN by hydrothermalsynthesis](#)
H Q Le, S J Chua, K P Loh *et al.*
- [Emission characteristics of ZnO nanorods on nanosilicon-on-insulator: competition between exciton-phonon coupling and surface resonance effect](#)
S K Mohanta, S Tripathy, C B Soh *et al.*
- [Zinc oxide nanorod based photonic devices: recent progress in growth, light emitting diodes and lasers](#)
M Willander, O Nur, Q X Zhao *et al.*

Recent citations

- [Study on optical properties of Ni@ZnO prepared by hydrothermal method](#)
Xiaoshuai Wu *et al*
- [Anomalous red emission with competition and coexistence of defect and band edge emission in photo-electrochemically active \(Zn_{0.97}Ga_{0.03}\)\(O_{0.95}N_{0.05}\) solid solution](#)
Sumithra Sivadas Menon *et al*
- [Novel photoluminescence properties and enhanced photocatalytic activities for V₂O₅-loaded ZnO nanorods](#)
Haihong Yin *et al*

Investigation of low-temperature excitonic and defect emission from Ni-doped ZnO nanoneedles and V-doped ZnO nanostructured film

Shubra Singh^{1,4}, Daisuke Nakamura², Kentaro Sakai³,
Tatsuo Okada² and M S Ramachandra Rao¹

¹ Department of Physics, Materials Science Research Centre and Nanofunctional Materials Technology Centre, IIT Madras, Chennai 600 036, India

² Department of Electrical Engineering, Kyushu University, Fukuoka 819-0395, Japan

³ Cooperative Research Center, University of Miyazaki, Miyazaki 889-2192, Japan

E-mail: shubra6@gmail.com

New Journal of Physics **12** (2010) 023007 (11pp)

Received 16 July 2009

Published 9 February 2010

Online at <http://www.njp.org/>

doi:10.1088/1367-2630/12/2/023007

Abstract. We report the growth and low-temperature photoluminescent characteristics of well-aligned Ni-doped ZnO nanoneedles and V-doped ZnO nanostructured thin film grown by a modified pulsed laser deposition technique. Low-temperature photoluminescence spectra of the as-grown films show the presence of free excitonic as well as bound excitonic transitions, whose relative intensity changes with increasing temperature. Ni-doped ZnO films show a characteristic fine structure in the visible range (2.6–2.9 eV) attributed to either exciton–polariton longitudinal–transverse splitting or the splitting caused by electron–hole exchange interaction. The excitonic and visible region emission can be clearly seen as can the phonon replicas produced from longitudinal optical phonons. Different possible attributions of the various peaks in the emission band at low temperature have been discussed. The as-grown nanostructures of Ni- and V-doped ZnO thin films also clearly show the effect of doping on the microstructure of ZnO.

⁴ Author to whom any correspondence should be addressed.

Contents

| | |
|---|-----------|
| 1. Introduction | 2 |
| 2. Experimental conditions | 2 |
| 3. Results and discussion | 3 |
| 3.1. Microstructure of as-grown films | 3 |
| 3.2. Investigation of low-temperature PL on as-grown thin films | 5 |
| 4. Conclusions | 10 |
| References | 11 |

1. Introduction

It has recently been shown that ZnO nanowires can be successfully used as active elements in nanoscale optical devices, such as photodetectors and lasers operating in the low-wavelength region [1, 2]. Such applications are also called for in the visible wavelength region. However, despite significant progress in nanowire device development, a detailed understanding of the effect of nanostructure size and morphology on their optical properties remains limited. The morphology and average size of nanocrystalline powders or films strongly depend on the preparation method and synthesis conditions. Photoluminescence (PL) from the as-prepared ZnO samples depends largely on defect content, stoichiometry, dopant type and concentration, grain size and powder morphology. Among the important dopants of the ZnO system, transition metal ions have received great attention because of their contribution toward the growth of ZnO-based diluted magnetic semiconductors. It is well known that the morphology of ZnO nanostructures is strongly dependent on experimental conditions [3]. These experimental conditions also affect the luminescent method, which is very sensitive to defect content, stoichiometry, impurity type and concentration, grain size and powder morphology. ZnO nanorods show different emission bands, depending on the doping material [4]. Pb²⁺-doped ZnO nanorods exhibited violet and blue emission bands [5]. V and Ni are also among the most efficient doping elements to improve and tune the optical, electrical and magnetic properties of ZnO nanomaterials [6]–[8]. Thus, the study of the optical properties of V- and Ni-doped ZnO is important from both the fundamental and applied points of view. Zhang *et al* [9] reported that doping of Ni leads to the increase of ultraviolet emission intensity and a blueshift of the emission peak. Contrary to this in the present work, we observe a suppression of the UV peak and an increase in defect emission. There have also been other reports on the room-temperature PL of Ni-doped ZnO rods [10, 11] as well as of Ni-doped ZnO films annealed at different temperatures [12, 13].

In the present paper, we report the synthesis, microstructure and room-temperature as well as low-temperature PL of V- and Ni-doped ZnO nanorods. The objective of this study is to see the effect of V and Ni doping on the microstructure and emission spectrum of ZnO. On the basis of theoretical analysis and observed interesting results, the origins of absorptions in the different wavelength regions at low-temperature emission are discussed in detail.

2. Experimental conditions

Ni-doped ZnO nanoneedles and V-doped ZnO nanostructured films were grown using a modified pulsed laser deposition (PLD) technique [14]–[16]. The modified PLD system can

Table 1. Deposition parameters for the growth of Ni- and V-doped ZnO films by a modified PLD setup.

| | |
|---------------------------------------|----------------------|
| Target | ZnO + V ZnO + Ni |
| Ablation time | 20 min |
| Chamber temp. | 1000 °C |
| Pressure | 260 Torr |
| Substrate | Sapphire(0001) |
| Distance between target and substrate | 1.5 cm |
| Laser | KrF excimer |
| Laser repetition rate | 20 Hz |
| Laser fluence | 4 J cm ⁻² |
| Pulse energy | 80 mJ |

sustain high temperature (as high as 1200 °C) and high pressure (~300 Torr), which assists in nanostructure formation. In our experiment, sintered ZnO:Ni and ZnO:V targets were used as source material in synthesizing ZnO nanowires. The sapphire substrate was inserted into a horizontal quartz tube chamber and the target–substrate distance was set to 15 mm. Then the chamber temperature was heated from room temperature to 1000 °C with a heating rate of 15 °C min⁻¹ and the chamber pressure filled with argon or nitrogen background gas was set to 260 Torr. The Ar or N₂ gas flow rate was set at 27.4 sccm. The ZnO target was ablated with a KrF excimer laser, which operates at a repetition rate of 20 Hz and a fluence of about 4 J cm⁻², in the chamber for 20 min. Ablated species were then deposited on substrates that had been pre-annealed at 1000 °C for 1 h in a programmable box-type electric-resistance furnace in order to improve the substrate surface condition and favor the aligned growth of ZnO nanowires. The deposition conditions are mentioned in table 1. Ni- and V-doped ZnO films were deposited in Ar as well as N₂ gas atmospheres. Phase analysis of the thin films was carried out using x-ray diffraction (XRD) (Rigakudenki MultiFlex). Scanning electron microscopy (model—Keyence VE-7800) measurements were performed to investigate the microstructure of as-grown films. For PL measurements, a He–Cd laser (325 nm) was used as the excitation source. A photomultiplier tube was used as the detector.

3. Results and discussion

3.1. Microstructure of as-grown films

Ni- and V-doped films grown in N₂ and Ar atmospheres have hexagonal wurtzite structure (as determined from XRD—figure 1). Figure 2 shows the scanning electron microscopy (SEM) images of Ni- and V-doped films grown in different atmospheres. Nanoneedles grown in Ar atmosphere have diameters of about 300 nm at the base, which taper down to 50 nm at the tip, and lengths up to 4 μm. Hence the resulting estimated aspect ratio is expected to vary from 14 at the base to about 80 at the tip. However, nanoneedles grown in N₂ atmosphere have a diameter of 200 nm at the base, 30 nm at the tip and lengths up to 2.5 μm on average.

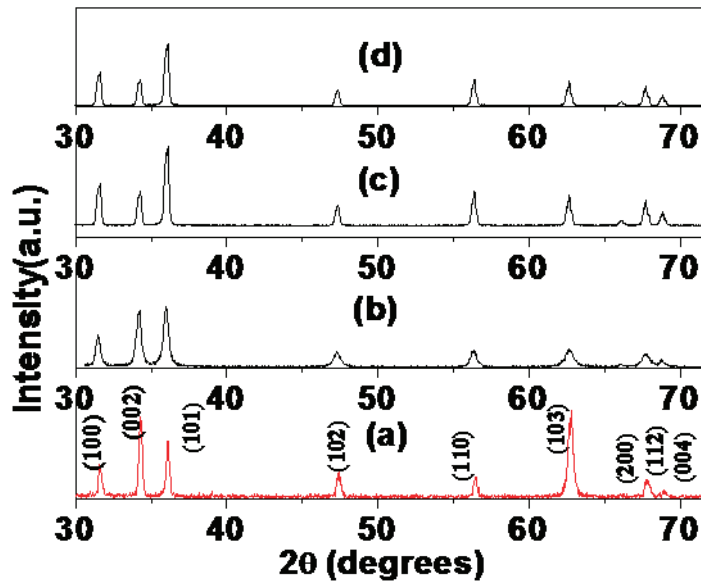


Figure 1. XRD patterns of as-grown Ni-doped ZnO film in (a) Ar, (b) N₂ and V-doped ZnO film in (c) Ar, (d) N₂.

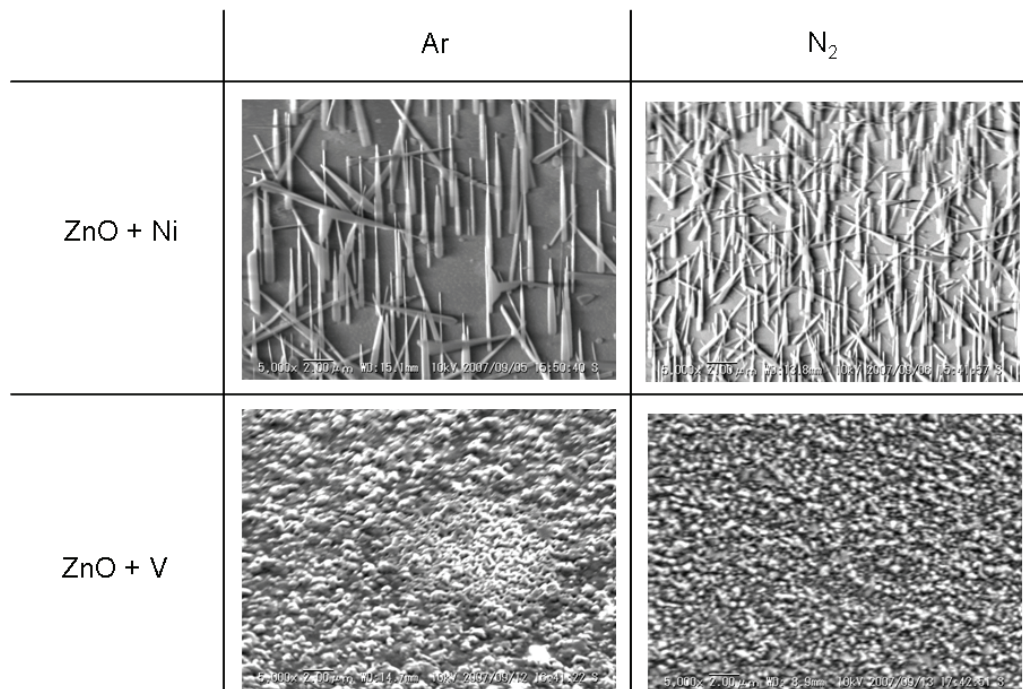


Figure 2. SEM images of Ni- and V-doped films grown in Ar and N₂.

V-doped thin films did not show any unique microstructure and the morphology was completely different from that of Ni-doped ZnO film. This clearly shows that different dopants can give rise to different microstructures of as-grown films. Doping with different TM ions (Ni or V) can dramatically affect the microstructure and optical properties of ZnO. A similar

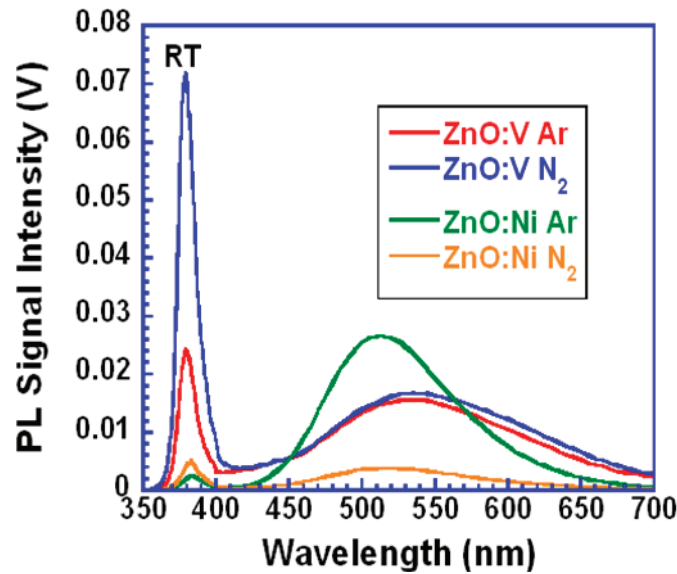


Figure 3. Room temperature PL spectra of Ni:ZnO and V:ZnO thin films grown in Ar and N₂ atmospheres.

effect has also been observed in the literature for Cr, Mo and W doping in bulk ZnO [17], where the morphology of the parent compound was altered by doping. The morphology of a compound depends on the ionic fraction of a compound, given by the following expression [18]:

$$16\Delta\chi + 3.5(\Delta\chi)^2,$$

where $\Delta\chi$ is the difference in electronegativity of the host element and the dopant element. Similar results have also been reported before for other growth techniques [19]. On obtaining SEM images at different spots on the film, the density of nanoneedles in the film was found to be different for different growth atmospheres. This could be attributed to the fact that the deposition rate for films grown in Ar is lower because of its heavier ionic mass, leading to a lower density of ZnO needles. This difference could also be due to the smaller mean free path of ablated species in the Ar atmosphere (due to the higher ionic radius of Ar) caused by a higher number of collisions of the species and thus larger nanostructure dimensions (as it seems from the comparison of SEM images) as well as lower density.

3.2. Investigation of low-temperature PL on as-grown thin films

PL spectroscopy is a powerful and nondestructive method to explore the optical characteristics of doped ZnO systems. Although room-temperature PL is essential for determining the optical applications of such materials, temperature-dependent PL can especially reveal the dissociation processes of impurity bound excitons induced by doping, and provide useful information. Hence the PL spectra of Ni- and V-doped ZnO films have been measured at different temperatures. The excitonic and visible region emission can be clearly seen as can the phonon replicas produced from longitudinal optical phonons.

The PL spectra of ZnO:Ni and ZnO:V (figure 3) exhibit UV emission as well as defect emission in the visible spectral range. From figure 3 it is clear that the ZnO:V sample shows

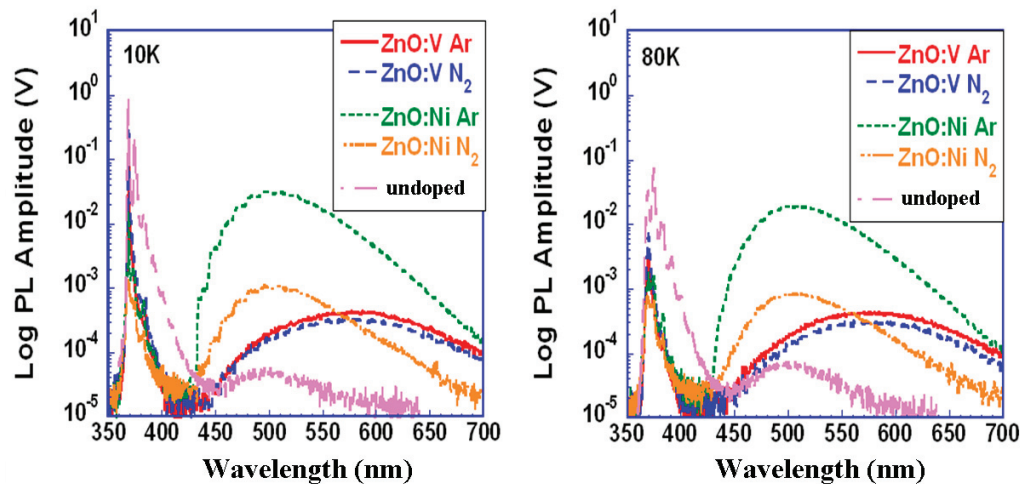


Figure 4. Low-temperature PL spectra of Ni:ZnO and V:ZnO thin films grown in Ar and N₂ atmospheres.

strong UV luminescence near 380 nm as compared to Ni-doped samples. The strength of UV luminescence depends on the relative concentration of the different species involved, their carrier trapping rates and also the ionization cross-section of the TM ion, which is different for each TM ion and also the host. The peak of defect level emission for the ZnO:V sample exists at about 530 nm and for the ZnO:Ni sample at 510 nm. This is attributed to the fact that the nature of native defects is different in both cases. The impurity levels of dopants in ZnO are different and are responsible for emission in the visible region. Each TM ion doping is found to affect the interface traps existing in the depletion regions between the ZnO–ZnO grain boundaries, giving rise to emission in the visible region. This is the reason for the strong defect level emission in doped samples as compared with undoped samples at temperatures of 10 and 80 K (figure 4). It is also clear that the area under deep level emission (in the visible region) and the range of defect emission increase on doping. This shows that there is an increase of vacancy and/or impurity concentration by doping. Ni and V doping also suppresses UV emission at about 380 nm, which indicates that TM ion doping increases the nonradiative recombination processes. TM ions are expected to act as killer centers to suppress transitions resulting in radiative recombination. These nonradiative transitions may arise when free electrons recombine via a TM ion impurity level instead of populating donor acceptor pairs and can also be attributed to energy transfer processes from donor–acceptor pairs to neighboring TM ions [20, 21]. Figure 5 shows the temperature dependence of defect level emission for V-doped ZnO grown in Ar and N₂ atmospheres. In general, the total integrated PL intensity usually decreases gradually with increasing temperature. This is usually due to several quenching mechanisms, such as thermal activation of some nonradiative centers. However, due to the presence of transition metal ion dopants (well known as killer centers) in the present samples, nonradiative centers are dominant at all temperatures. This may explain the absence of a significant decrease in PL intensity of the band with increase in temperature. We find that the defect level peak position for V-doped ZnO shifts from 580 to 530 nm with increase in sample temperature. Such large shifts between the PL energy peaks and the shape of the PL emission bands are signatures of deep levels with strong electron–phonon coupling [22].

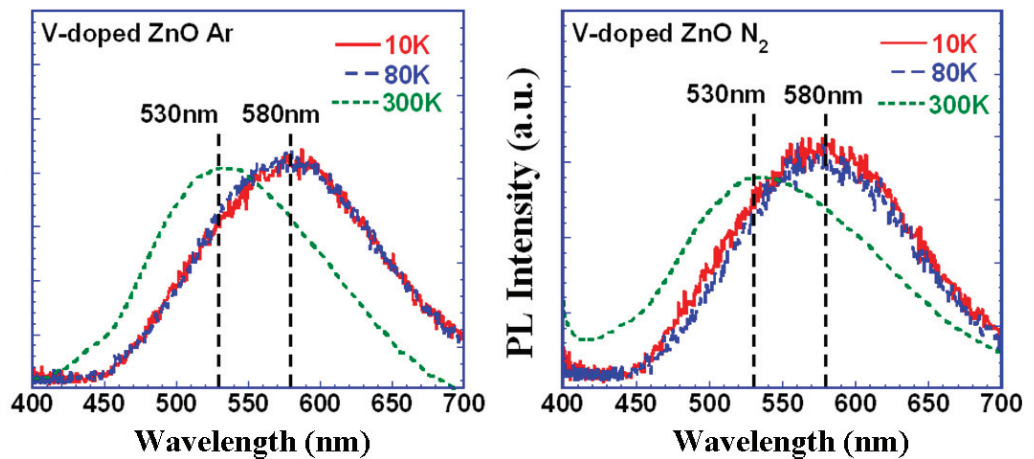


Figure 5. Temperature dependence of visible emission from V-doped samples.

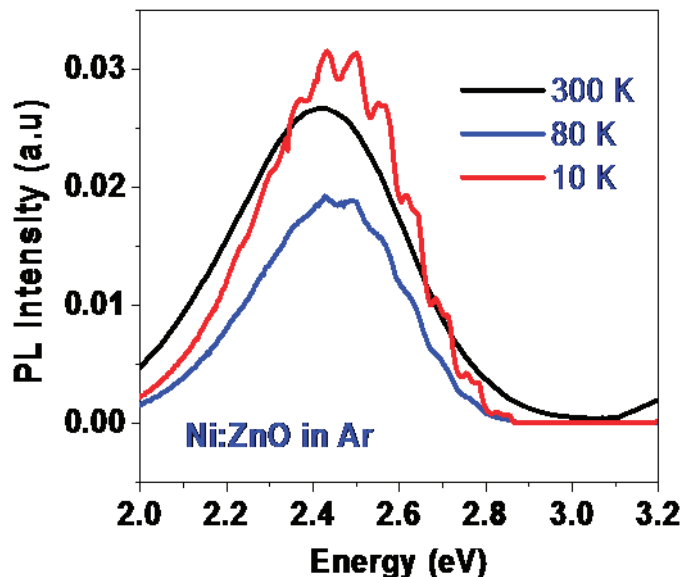


Figure 6. Temperature dependence of visible spectra of Ni:ZnO films grown in Ar atmosphere.

Similar results have been observed by Shi *et al* [23]. Shi *et al* observed that the peak position of the emission band remains unchanged when the temperature is not higher than 200 K (similar to our case). For high temperatures, the peak position tends to blue shift with increasing temperature. This phenomenon has been explained as being a result of populating the higher vibronic states at higher temperatures. The nature of the centers responsible for these emission bands and related recombination mechanisms are not still understood, and call for further investigations.

Figure 6 shows the plot of the low-temperature PL spectrum at 10–300 K for Ni-doped ZnO grown in the visible range in Ar atmosphere. The plot shows a characteristic fine structure in the visible range (2.6–2.9 meV). The fine structure observed in the visible range of the PL

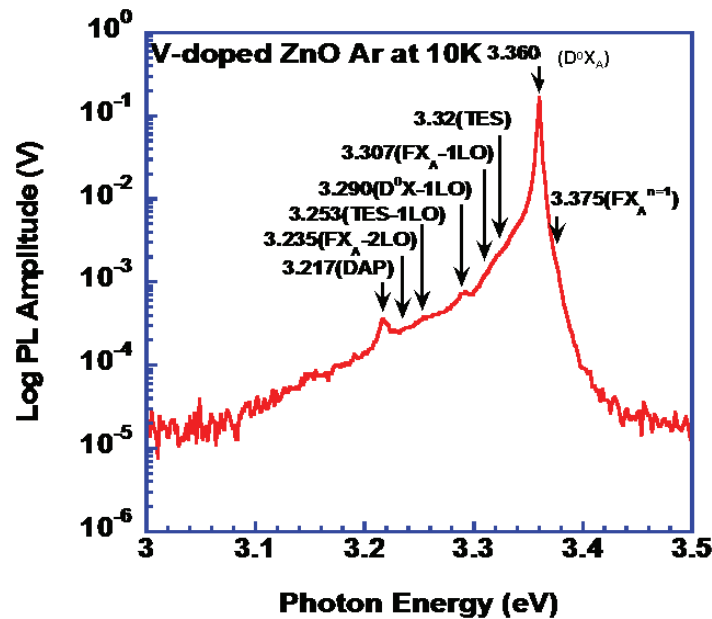


Figure 7. Logarithmic plot of the low-temperature PL spectrum of V:ZnO films grown in Ar atmosphere at 10 K.

spectrum at 10 K in the present paper is very similar to the fine structure observed in the visible range of the low-temperature PL spectra of Cu-doped ZnO films [24]. Indeed, in both cases, a zero-phonon peak (constituted by two close lines) is observed in the high-energy side of the defect band, and its phonon replicas are present at lower energies. These features were attributed to the defect energy levels introduced inside the ZnO energy gap by the Cu dopant. Due to the high similarity of these features in the two cases (the structure constituted by the two lines forming the zero-phonon peak can be observed by a slight magnification of the PL spectrum in the visible range of Ni-doped ZnO in figure 6), it can be thought that the effect of Ni doping is similar to that caused by Cu doping. The spectrum of annealed Cu-doped ZnO nanowires at low temperature (10 k) has been seen to exhibit a red shift in UV and blue emission relating to the different valence states of Cu atoms in ZnO [25, 26].

However, the lack of this fine structure in V-doped ZnO can be due to a possible different incorporation of V inside ZnO, which does not give rise to the same fine structure. We would also like to mention that the fine structures fade out gradually with increasing temperature and are no longer observable when the temperature is 300 K. This may be attributed to the thermal broadening of each vibronic transition [23].

The wurtzite ZnO conduction band is mainly constructed from the s-like state, whereas the valence band is a p-like state, which is split into three bands due to the influence of crystal-field and spin-orbit interactions [27]. The near-band-gap intrinsic absorption and emission spectrum is therefore dominated by transition from these three valence bands. The related free exciton transitions from the conduction band to these three valence bands or vice versa are usually denoted by A (also referred to as the heavy hole), B (also referred to as the light hole) and C (also referred to as crystal-field split band).

Figure 7 shows the low-temperature PL spectrum of ZnO:V films grown in Ar atmosphere at 10 K. At such low temperatures the A free exciton transition is observed at $FX_A = 3.375$ eV

[28, 29]. Bound excitons are extrinsic transitions and are related to dopants or defects, which usually create discrete electronic states in the band gap, and therefore influence both optical absorption and emission processes. The electronic states of bound excitons depend strongly on the semiconductor material, in particular, the band structure. In theory, excitons could be bound to neutral or charged donors and acceptors. A basic assumption in the description of bound exciton states for neutral donors and acceptors is a dominant coupling of like particles in the bound exciton states. These two classes of bound excitons are by far the most important cases for direct band-gap materials. In high-quality bulk ZnO, the neutral shallow donor bound exciton (DBE) often dominates because of the presence of donors due to unintentional (or doped) impurities and/or shallow donor-like defects. In samples containing acceptors, an acceptor bound exciton is observed. In the low-temperature PL for the V-doped sample, we observe a prominent line, which is the A exciton bound to a neutral donor, positioned at 3.36 eV (D_0X_A). It has a full-width at half-maximum of about 0.7 meV, indicating good quality of the sample. Based on the energy separation between the FX_A and DBE peak, it is concluded that the binding energy of the DBE related to the donor is 15 meV. The PL spectrum at 10 K is dominated by neutral donor bound exciton emissions.

Another characteristic of the neutral donor bound exciton transition is the two-electron satellite (TES) transition in the spectral region of 3.32–3.34 eV. The main peak at 3.32 eV ($(D_0X_A)_e$) is the excited state associated with the most intense neutral donor bound exciton at 3.36 eV (D_0X_A). These transitions involve radiative recombination of an exciton bound to a neutral donor, leaving the donor in the excited state, thereby leading to a transition energy that is less than the DBE energy by an amount equal to the energy difference between the first excited and ground states of the donor. In the effective-mass approximation, the energy difference between the ground-state neutral donor bound excitons and their excited states (TES) can be used to determine the donor binding energies [30, 31]. The donor excitation energy from the ground state to the first excited state is equal to 3/4 of the donor binding energy E_D . Hence the donor binding energy turns out to be 53 meV for the donor at 3.36 eV.

The spectral region containing the donor–acceptor pair (DAP) transition and LO-phonon replicas of the main transitions has not been studied widely for single-crystal ZnO. It should be noted that LO-phonon replicas occur with a separation of 71–73 meV, the LO-phonon energy in ZnO [32]. The peak at 3.307 eV is the first phonon replica of the free exciton peak $FX_A = 3.375$ eV and the peak at 3.235 is its second phonon replica (FX_A-2LO). The peak at 3.29 eV is the first phonon replica ((D_0X_A-1LO)) of 3.360 eV (D_0X_A). Teke *et al* [33] observed a radiative recombination peak at 3.217 eV, which is attributed to the donor–acceptor pair labeled as the DAP transition. The peak at 3.253 eV is the phonon replica of 3.32 eV ($(D_0X_A)_e$).

Figure 8 shows the low-temperature PL spectrum of Ni:ZnO grown in Ar atmosphere at 10 K. We do not observe any acceptor bound exciton peak, which generally occurs at around 3.356 eV [34]. Figure 9 shows the temperature dependence of excitonic emission in the PL spectra of Ni:ZnO. From figure 9 it is clear that the relative intensity ratio I_F/I_B (intensity of free exciton FX_A /intensity of bound exciton (D_0X_A)) increases with increase in temperature, showing that with increasing temperature the dominant DBE dissociates into a free exciton and a neutral donor [35]. We observe a similar effect in the free to bound exciton intensities for V:ZnO.

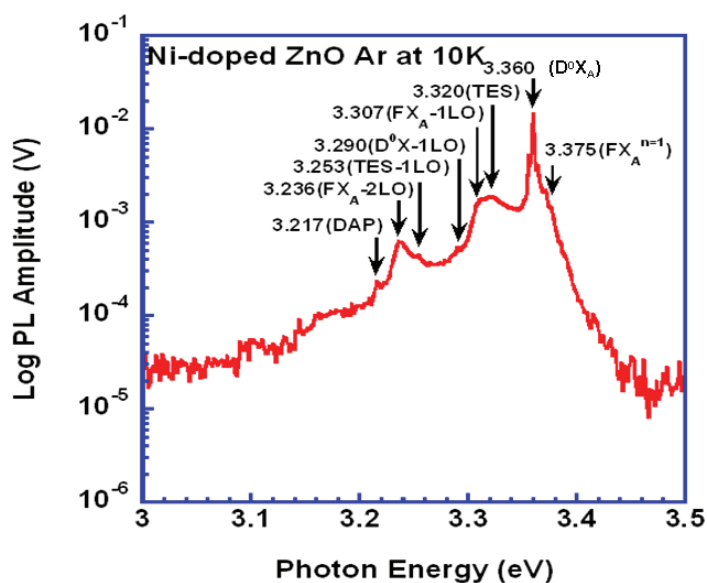


Figure 8. Logarithmic plot of the low-temperature PL spectrum of Ni:ZnO grown in Ar atmosphere at 10 K.

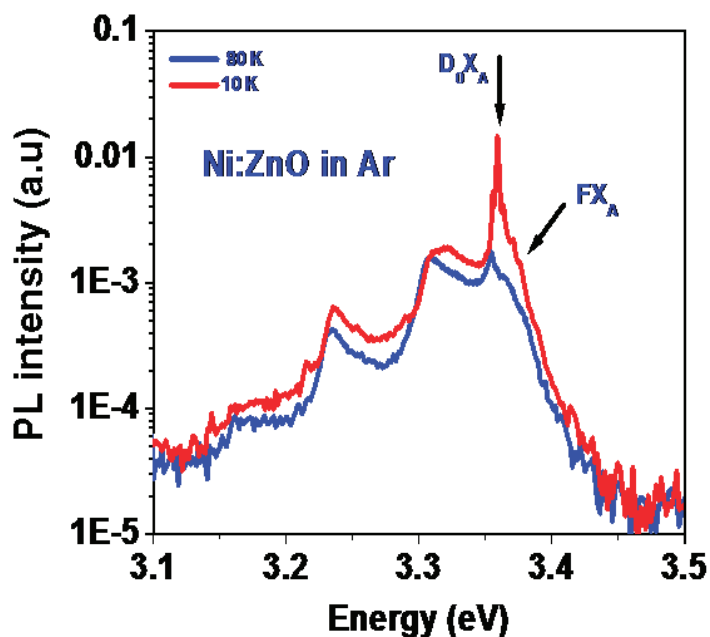


Figure 9. Temperature dependence of excitonic emission in the PL spectra of Ni:ZnO.

4. Conclusions

Ni-doped ZnO nanoneedles and V-doped ZnO nanostructures were grown by a modified PLD setup. Two different dopants gave rise to different microstructures of the as-grown films attributed to the change in electronegativity of the dopant element with respect to the doped element. The clear difference in the nature of deep level emission from doped films proved that the nature of native defects is different in each case. Low-temperature PL spectra of the films

show the presence of free excitons as well as neutral donor bound excitonic transitions. The relative intensity ratio I_F/I_B (intensity of free exciton FX_A /intensity of bound exciton (D_0X_A)) increases with increase in temperature, showing that with increasing temperature the dominant DBE dissociates into a free exciton and a neutral donor.

References

- [1] Hsu C-L, Hsueh T-J and Chang S-P 2008 *J. Electrochem. Soc.* **155** K59–62
- [2] Bagnall D M, Chen Y F, Zhu Z, Yao T, Koyama S, Shen M Y and Goto T 1997 *Appl. Phys. Lett.* **70** 2230
- [3] Guo M, Diao P and Cai S 2005 *J. Solid State Chem.* **178** 1864
- [4] Bae S Y, Na C W, Kang J H and Park J 2005 *J. Phys. Chem. B* **109** 2526
- [5] Chu D, Zeng Y P and Jiang D 2006 *Mater. Lett.* **60** 2783
- [6] Saeki H, Tabata H and Kawai T 2001 *Solid State Commun.* **120** 439–43
- [7] Wakano T, Fujimura N, Morinaga Y, Abe N, Ashida A and Ito T 2001 *Physica E* **10** 260–4
- [8] Shimono D, Tanaka S, Torikai T, Watari T and Murano M 2001 *J. Ceram. Proc. Res.* **2** 184–8
- [9] Zhang B, Zhang X-T, Gong H-C, Wu Z-S, Zhou S-M and Du Z-L 2008 *Phys. Lett. A* **372** 2300–3
- [10] Wu D, Yang M, Huang Z, Yin G, Liao X, Kang Y, Chen X and Wang H 2009 *J. Colloid Interface Sci.* **330** 380–5
- [11] He H Jr, Lao C S, Chen L J, Davidovic D and Wang Z L 2005 *J. Am. Chem. Soc.* **127** 16376–7
- [12] Qiu D J, Wu H Z, Feng A M, Lao Y F, Chen N B and Xu T N 2004 *Appl. Surf. Sci.* **222** 263–8
- [13] Iqbal J, Wang B, Liu X, Yu D, He B and Yu R 2009 *New J. Phys.* **11** 063009
- [14] Okada T, Agung B H and Nakata Y 2004 *Appl. Phys. A* **79** 1417
- [15] Okada T, Kawashima K, Nakata Y and Ning X 2005 *Japan. J. Appl. Phys.* **44** 688
- [16] Okada T, Kawashima K and Nakata Y 2006 *Thin Solid Films* **506–507** 274
- [17] Sato T, Suzuki H, Kido O, Kurumada M, Kamitsuji K, Kimura Y, Kawasaki H, Kaneko S, Saito Y and Kaito C 2005 Production of transition metal-doped ZnO nanoparticles by using RF plasma field *J. Cryst. Growth* **275** e983
- [18] Blinder S M 2003 *Introduction to Quantum Mechanics in Chemistry, Materials Science and Biology* (Amsterdam: Elsevier Academic)
- [19] Li D, Liu Z T, Leung Y H, Djurišić A B, Xie M H and Chan W K 2008 *J. Phys. Chem. Solids* **69** 616
- [20] Godlewski M 1983 *Solid State Commun.* **47** 811
- [21] Godlewski M and Skowronski M 1985 *Phys. Rev. B* **32** 4007
- [22] El Mir L, El Ghoul J, Alaya S, Ben Salem M, Barthou C and von Bardeleben H J 2008 *Physica B* **403** 1770
- [23] Shi S L, Li G Q, Xu S J, Zhao Y and Chen G H 2006 *J. Phys. Chem. B* **110** 10475–8
- [24] Dingle R 1969 *Phys. Rev. Lett.* **23** 579
- [25] Zhu H, Iqbal J, Xu H and Yu D 2008 *J. Chem. Phys.* **129** 124713
- [26] Zhang Z *et al* 2008 *J. Phys. Chem. C* **112** 9579–85
- [27] Mang A, Reimann K and Rübenacke St 1995 *Solid State Commun.* **94** 251
- [28] Xiang B, Wang P W, Zhang X Z, Dayeh S A, Aplin D P R, Soci C, Yu D P and Wang D L 2007 *Nano Lett.* **7** 323
- [29] Shan C X, Liu Z and Hark S K 2008 *Appl. Phys. Lett.* **92** 073103
- [30] Thonke K, Gruber T, Teofilov N, Schönfelder R, Waag A and Sauer R 2001 *Physica B* **308–310** 945
- [31] Alves H, Pfisterer D, Zeuner A, Riemann T, Christen J, Hofmann D M and Meyer B K 2003 *Opt. Mater* **23** 33
- [32] Wang L and Giles N C 2003 *J. Appl. Phys.* **94** 973
- [33] Teke A, Özgür Ü, Doğan S, Gu X, Morkoç H, Nemeth B, Nause J and Everitt H O 2004 *Phys. Rev. B* **70** 195207
- [34] Özgür Ü, Alivov Ya I, Liu C, Teke A, Reshchikov M A, Doğan S, Avrutin V, Cho S-J and Morkoç H 2005 *J. Appl. Phys.* **98** 041301
- [35] Viswanath A K, Lee J I, Kim D, Lee C R and Leem J Y 1998 *Phys. Rev. B* **58** 16333–9